Earth and Planetary Science Letters 519 (2019) 234–244

Contents lists available at ScienceDirect

Earth and Planetary Science Letters

www.elsevier.com/locate/epsl

Barium-isotopic constraints on the origin of post-Marinoan barites

Peter W. Crockford [a,b,*], Boswell A. Wing [c], Adina Paytan [d], Malcolm S.W. Hodgskiss [e], Kimberley K. Mayfield [d], Justin A. Hayles [f], Julia E. Middleton [g], Anne-Sofie C. Ahm [b], David T. Johnston [h], Fabricio Caxito [i], Gabriel Uhlein [i], Galen P. Halverson [j,k], Benjamin Eickmann [l], Marta Torres [m], Tristan J. Horner [g]

[a] Department of Earth and Planetary Science, Weizmann Institute of Science, Rehovot 76100, Israel
[b] Department of Geosciences, Princeton University, Princeton NJ 08544, USA
[c] Department of Geological Sciences, University of Colorado Boulder, Boulder, CO 80309, USA
[d] Institute of Marine Science, University of California–Santa Cruz, Santa Cruz, CA 95064, USA
[e] Department of Geological Sciences, Stanford University, Stanford CA 94305, USA
[f] Department of Earth, Environmental and Planetary Sciences, Rice University, Houston TX, USA
[g] Department of Marine Chemistry, Woods Hole Oceanographic Institution, Woods Hole MA, USA
[h] Department of Earth and Planetary Science, Harvard University, Cambridge MA 02138, USA
[i] CPMTC – IGC – Universidade Federal de Minas Gerais, Belo Horizonte 31270-901, Brazil
[j] Department of Earth and Planetary Sciences, McGill University, Montréal QC H3A 0E8, Canada
[k] Earth Dynamics Research Group and The Institute for Geoscience Research (TIGeR), School of Earth and Planetary Sciences, Curtin University, GPO Box U1987, WA 6845, Australia
[l] Department of Geosciences, University of Tübingen, Germany
[m] College of Earth, Ocean and Atmospheric Sciences, Oregon State University, USA

ARTICLE INFO

Article history:
Received 2 December 2018
Received in revised form 2 May 2019
Accepted 8 May 2019
Available online 29 May 2019
Editor: L. Derry

Keywords:
barium isotopes
Snowball Earth
barite
cryogenian
barium cycle
Marinoan

ABSTRACT

Measurements of triple oxygen isotope ratios in barite horizons within post-Marinoan cap carbonates have provided some of the most compelling evidence that the Marinoan glaciation was a Snowball Earth event. However, the origin of these barite horizons remains unresolved. To constrain the Ba sources, and thus formation mechanisms of these horizons, we analyzed the Ba isotope composition of post-Marinoan barite deposits from Northwest Canada, Northern Norway, Brazil and South China. We augment these analyses with a Ba isotope survey of almost 100 modern and ancient additional barite measurements, including samples from pelagic (or 'marine'), hydrothermal, terrestrial, Proterozoic stratiform and cold seep environments. Unlike modern cold seep or terrestrial barites, we find that globally-distributed post-Marinoan barites exhibit a relatively narrow isotopic range, suggesting a well-mixed, effectively limitless Ba source. Moreover, post-Marinoan deposits exhibit a similar mean Ba isotope composition to modern marine barites, which we interpret as evidence of a marine Ba source. Considered alongside existing geochemical, geological, and new Ba isotope survey data, we conclude that Ba in barite horizons was sourced from a well-mixed, Ba-replete but SO_4-poor reservoir that accumulated during the Marinoan Snowball Earth interval. This deep Ba reservoir was then transported upward—either by ocean circulation or dolomitization of underlying cap carbonates—and was brought into contact with continental weathering-derived sulfate in a post-glacial meltwater surface layer. Thus, in addition to providing a plausible mechanism for generating globally-synchronous deposition of post-Marinoan barite horizons that reconciles all existing geochemical and geological data, our results demonstrate the utility of Ba isotopes to interrogate the origin of enigmatic barite deposits throughout the sedimentary record.

1. Introduction

Barite ($BaSO_4$) cements deposited in the aftermath of the Marinoan glaciation (ca. 635 Ma) bear some of the most important geochemical evidence in support of a Neoproterozoic Snowball Earth (Bao et al., 2008). Central to the Snowball Earth hypothesis is the prediction of a large syn-glacial build-up of atmospheric CO_2 (pCO_2; >100 × preindustrial atmospheric levels) due to a shutdown of chemical weathering but continued volcanic CO_2 degassing on an ice-covered planet (Kirschvink, 1992). Such high concentrations of atmospheric CO_2 would be required to overcome the

* Corresponding author.
E-mail address: peter.crockford@weizmann.ac.il (P.W. Crockford).

https://doi.org/10.1016/j.epsl.2019.05.018
0012-821X/

effect of a high planetary albedo and trigger catastrophic termination of the Snowball climate state. Seafloor barite cements, which are unique to Marinoan post-glacial sequences, preserve critical evidence for this prediction of an extremely elevated pCO_2 climate state through negative triple oxygen isotope anomalies (Bao et al., 2008; Cao and Bao, 2013; Crockford et al., 2016, 2018a).

Negative triple oxygen isotope anomalies ($\Delta^{17}O = \ln[\delta^{17}O + 1] - 0.5305 \ln[\delta^{18}O + 1]$) are mass-independent depletions of oxygen isotopes within atmospheric O_2 or other oxy-anions such as sulfate (SO_4^{2-}). The $\Delta^{17}O$ value of tropospheric oxygen is primarily governed by atmospheric chemistry (predominantly pO_2 and pCO_2 levels) and the biospheric flux of O_2 into the atmospheric reservoir (Luz et al., 1999). In the ancient atmosphere, anomalously negative $\Delta^{17}O$ values well below those of modern tropospheric O_2 ($\Delta^{17}O = -0.516‰$; Pack et al., 2017), could have been generated in two different ways that are not mutually exclusive. First, extremely high concentrations of atmospheric CO_2 interact with oxygen radicals during the photo-dissociation of stratospheric ozone (O_3) that bear a positive $\Delta^{17}O$ signature. These reactions allow for O_2 involved in ozone dissociation reactions to exit the stratosphere with a large negative $\Delta^{17}O$ value that scales with pCO_2 levels (Wen and Thiemens, 1993). A second mechanism to generate large depletions in $\Delta^{17}O$ values of tropospheric O_2 is to reduce the rate of O_2 production via photosynthesis (Crockford et al., 2018b, 2019). This factor arises because anomalous $\Delta^{17}O$ values generated in the stratosphere are diluted in the troposphere by O_2 produced via photosynthesis, which sources oxygen from seawater ($\Delta^{17}O = 0‰$). Therefore, reducing the photosynthetic O_2 flux essentially cedes a greater proportional influence to stratospheric chemistry by increasing the O_2 residence time (modern = 1400 yrs; Bender et al., 1994), and, in turn, results in a negative $\Delta^{17}O$ anomaly in the tropospheric reservoir (Cao and Bao, 2013). These processes then have the potential to be recorded within local or possibly global SO_4 reservoirs that capture a portion of the atmospheric signal during pyrite oxidation provided subsequent microbial sulfur cycling does not erase atmospheric signatures through oxygen exchange with water (cf. Crockford et al., 2016, 2018b, 2019). Such signals can then be preserved within the sedimentary record if the SO_4^{2-} produced via O_2-oxidation of reduced sulfur reacts with a cation such as barium (Ba^{2+}) and is preserved as a SO_4-bearing mineral such as barite within the sedimentary record (Bao et al., 2008).

Post-Marinoan barite horizons have now been documented in seven regions globally, five of which preserve large negative $\Delta^{17}O$ anomalies (i.e., below −0.5‰; Bao et al., 2008; Crockford et al., 2016, 2018a). During the aftermath of the Marinoan Snowball Earth, vigorous continental weathering likely led to high rates of primary productivity due to a high continentally derived nutrient flux to the oceans (Kunzmann et al., 2013). These observations, coupled to the $\Delta^{17}O$ anomalies, provide compelling evidence for extremely elevated levels of CO_2 at the time of the Marinoan deglaciation (Cao and Bao, 2013). Despite the crucial role of these post-Marinoan barites in substantiating the Neoproterozoic Snowball Earth hypothesis, the process by which these chemical sediments were deposited remains unresolved.

Two issues persist regarding the origin of post-Marinoan barites: how are atmospheric signals imparted to marine SO_4, and how did the barites that preserve these signals form? While many studies have focused on the former issue, with particular attention toward the origins and interpretations of oxygen ($\Delta^{17}O$) and sulfur ($\delta^{34}S$, $\Delta^{33}S$) isotope data within SO_4 (Shields et al., 2007; Bao et al., 2008; Peng et al., 2011; Killingsworth et al., 2013; Crockford et al., 2016), the question of Ba source has remained largely unaddressed. As a consequence, no holistic hypothesis has been developed for why such horizons exclusively formed during the aftermath of the second Cryogenian Snowball Earth glaciation (the Marinoan; ≈635 Ma; Hoffman et al., 2017 and references therein) and not the aftermath of the older and longer-lived Sturtian glaciation (≈659 Ma; Hoffman et al., 2017 and references therein). Moreover, post-Marinoan barites are the only globally isotopically correlative barite deposits known in the sedimentary record, making their origins, global distribution and preservation particularly enigmatic (Crockford et al., 2018a). Recent developments in Ba stable isotope mass spectrometry (e.g., Horner et al., 2015, 2017; Hsieh and Henderson, 2017; Bridgestock et al., 2018) have established an isotopic framework for deducing the source of Ba in sedimentary barites. We explore the deposition of the post-Marinoan horizons by reporting new Ba isotope data for these barites and compare results to an extensive survey of modern barites from a variety of settings (terrestrial, hydrothermal, cold seep and pelagic core-tops; Paytan et al., 1993, 1996; Paytan and Griffith, 2007; Griffith et al., 2018) along with older Proterozoic stratiform barites that have been suggested as analogues for modern cold seep environments (Torres et al., 2003). These new Ba-isotope data are presented and interpreted alongside existing sulfur ($\delta^{34}S$, $\Delta^{33}S$) and oxygen ($\delta^{18}O$, $\Delta^{17}O$) isotopic data of coeval SO_4 to discriminate between different models for barite formation. We conclude that the source of Ba to post-Marinoan barite was a deep homogeneous marine Ba pool in an ocean that remained stratified for $\approx 10^4$ yrs following deglaciation (Liu et al., 2014; Crockford et al., 2016; Yang et al., 2017). Using this model, we explore why such conditions may not have existed for the older and longer-lived Sturtian glaciation.

2. Barite formation models

Barite deposits in sedimentary environments represent the nexus of Ba- and SO_4-bearing solutions. Typically, one fluid contains Ba derived from the leaching of silicates, and the other is enriched in SO_4 (most often seawater). Provided that the mixture of these solutions rises above saturation (i.e., $\Omega_{barite} > 1$, where Ω_{barite} is the saturation state of the solution with respect to barite), barite precipitation is favored. Thus, the existence of a barite deposit is evidence for intense local disequilibrium due to either: (i) focused mixing of two separate crustal fluids (if the deposits were formed *in situ*), or (ii) precipitation within microenvironments that allow for local super saturation in undersaturated waters (e.g., Horner et al., 2017; Martinez-Ruiz et al., 2019). Several models have been proposed for the genesis of sedimentary barite deposits; broadly, each of these models represents a variant of these two formation scenarios. In the first class of models, barite formation occurs *in situ* at the intersection of distinct Ba- and SO_4-rich fluids. There are several modern analogues for similar mixing environments, such as cold seeps, continental runoff (rivers or subterranean groundwater discharge), hot springs, and hydrothermal vents. These mechanisms, along with other hydrologically-controlled scenarios, perhaps unique to the post-Marinoan world, are potentially identifiable using Ba isotopes, since different Ba sources possess distinct Ba isotope compositions (e.g., Horner et al., 2017). In the second class of models, local disequilibrium drives barite precipitation in focused microenvironments within a larger barite-undersaturated environment (e.g., Chow and Goldberg, 1960; Horner et al., 2017; Martinez-Ruiz et al., 2019). Indeed, this latter style of barite precipitation, termed 'pelagic' (or 'marine'), is ubiquitous in the modern ocean and likely drives much of the open marine Ba cycle (e.g., Chow and Goldberg, 1960; Dickens et al., 2003; Paytan and Griffith, 2007). Below, we outline competing scenarios that can reconcile existing S- and O-isotope geochemical observations that constrain the source of SO_4 to post-Marinoan deposits.

Table 1
Schematic models with descriptions and geochemical predictions of barite formation. In the top row a groundwater source of Ba is outlined. In this schematic model, Ba is released from Mn(O,OH) as salinity increases during marine transgression (blue line). In the middle row a cold seep model of barite precipitation is outlined. In this second model, Ba concentrations increase as the SO_4–CH_4 transition zone rises to the sediment water interface. In the bottom row a marine source of Ba is outlined. In this third model, Ba-rich seawater upwells or circulates through the sediment to meet SO_4-rich waters in the overlying meltwater lens. (For interpretation of the colors in the figure(s), the reader is referred to the web version of this article.)

Hypothesis	Source of Ba	Geochemical Predictions	Schematic
Barite forms as a result of Ba being desorbed from Mn-(hydr)oxides due to an increase in salinity in the subterranean estuary and then reacting with SO_4-rich overlying waters	Coastal	Ba isotopes should reflect a terrestrial source of Ba and show a high degree of variability due to a wide range of processes and local conditions in different locations	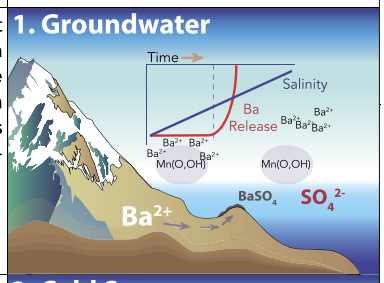
Barite forms from barium remobilized from pelagic barites deposited in productive waters, as an upward migration of the SMTZ allows for Ba to be released into SO_4-rich waters	Cold seep	Ba isotopes should show a wide range of values due to non-quantitative remobilization of Ba and isotopic heterogeneity along different margins due to diachronous deposition of initial pelagic barites	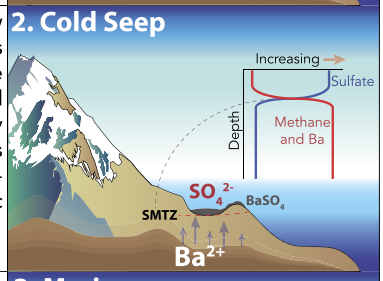
Barite forms when Ba-rich marine waters are either upwelled along margins upon breakdown of post-glacial stratification or as cap dolostones are dolomitized and released from Ba-rich limestones or dolomitizing fluids	Marine	Ba isotopes should show a similar range and value in all locations and this value and range should be similar to modern pelagic barites	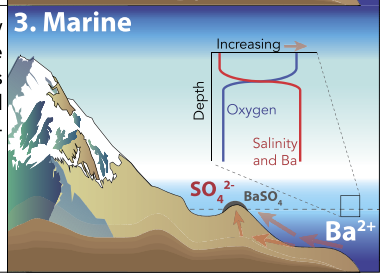

2.1. Cold seep

The earliest described model for post-Marinoan barite precipitation suggested formation in an environment analogous to modern cold seeps (Shields et al., 2007). Cold seep barite forms atop the sediment-water interface, typically underlying highly productive waters where CH_4 (methane) production outpaces the influx of SO_4 from overlying waters. When SO_4 is sufficiently consumed through microbial SO_4-reduction and anaerobic CH_4-oxidation, ambient Ω_{barite} will fall; once <1, barite within the sediment pile—built up along margins over thousands to potentially millions of years—starts to dissolve and Ba is remobilized (Riedinger et al., 2006). When this SO_4–CH_4 transition zone (SMTZ) is located near the sediment water interface, CH_4- and Ba-rich pore-fluids encounter seawater that is rich in SO_4, which leads to barite precipitation (Torres et al., 1996; Riedinger et al., 2006). If post-Marinoan barites formed in a similar manner (as has been suggested for Proterozoic stratiform deposits; Torres et al., 2003), it would require significant Ba accumulation in sediments and ample organic matter (or abundant gas-hydrate CH_4; Shields et al., 2007) to consume SO_4 within sediments. Accordingly, precipitates formed at cold seeps are expected to show a wide range of Ba isotope compositions owing to possible fractionation during diffusive transport (e.g., van Zuilen et al., 2016), non-quantitative dissolution and (re)precipitation of barite (Table 1), as well as potential variability in the Ba-isotope composition of the source barites themselves (Bridgestock et al., 2018, 2019). A possible challenge in applying a cold seep model to post-Marinoan deposits relates to this variability in global cold seep environments, where factors such as sediment deposition history, type, accumulation rate and microbial activity, make it unlikely that Ba release would occur in a globally-synchronous manner (i.e., within the age resolution for the globally distributed post-Marinoan barite horizons).

2.2. Coastal discharge

A second model suggests terrestrially derived fluids bearing elevated Ba concentrations, such as rivers or groundwater, reacted with relatively SO_4-rich seawater to precipitate post-glacial barite. Such a model for the formation of barite involves the geochemical dynamics at the redox interface between meteoric groundwater and seawater-derived SO_4. This interface, termed the subterranean estuary, allows for the buildup of Ba concentrations orders of magnitude above ambient pore-waters due to the adsorption of Ba onto Mn-(hydr)oxides (Charette et al., 2005). The stability of Ba sorbed to Mn-(hydr)oxides is dictated by pore-water salinity, pE and pH (Gonneea et al., 2013). Changes in these variables can cause desorption of Ba and release into solution (Table 1). While modern systems will typically precipitate barite within sediment matrices due to a redoxcline well below the sediment water interface, in the special case of the post-Marinoan ocean, the redoxcline may have approached the sediment water interface on continental shelves during the extreme post-glacial transgression with rapid melting of continental ice sheets and thermal expansion of waters.

From an isotopic standpoint, this formation mechanism is difficult to confidently constrain without comprehensive assessments of Ba isotopes in groundwater. However, it is possible to make some predictions (Table 1) based on existing data for rivers (e.g., Cao et al., 2016), coastal discharge (e.g., Bitterwolf et al., 2017), and terrestrially sourced barites (von Allmen et al., 2010), all of which show considerable spatial Ba isotope variability. Accordingly, barites formed via this mechanism are unlikely to exhibit similar Ba isotope compositions at multiple localities owing to differences in the local terrestrially derived Ba source.

2.3. Marine

A third model of post-Marinoan barite formation relies upon the formation of a deep anoxic water mass underneath an ice-covered ocean (Zhou et al., 2010). While no directly analogous scenario exists in the modern open ocean, high Ba concentrations are typically observed in anoxic portions of semi-restricted basins, such as the Cariaco Trench, Framvaren Fjord, and Black Sea (Falkner et al., 1993). In the case of the Marinoan, exhaustion of SO_4 from seawater due to microbial and hydrothermal SO_4-reduction during the Snowball glaciation coupled with limited oxidative weathering of sulfides on the continents, would lower marine Ω_{barite}. In turn, this would allow a large Ba reservoir to develop in the subglacial ocean from non-terrestrial Ba inputs (e.g., seafloor weathering and deep-sea hydrothermal fluxes) until Ω_{barite} once again approached unity. Resumption of continental weathering upon deglaciation would supply fresh SO_4 to the surface ocean that would, upon mixing with Ba-rich deep seawaters (for example in zones of upwelling, during dolomitization with Ba-rich seawater, or at the interface of these waters in certain locations), precipitate barite along continental margins until post-glacial destratification occurs (Hurtgen et al., 2006; Bao et al., 2008; Ahm et al., 2019; summarized in Crockford et al., 2016). Unlike the cold seep and terrestrial models described above, the central Ba-isotopic prediction of this model is that all contemporaneous barite deposits should exhibit a similar Ba-isotopic composition, since all of the Ba was sourced from an isotopically-homogeneous and effectively infinite Ba reservoir (Table 1). This model also allows for the synchronous initiation of this process globally or, at least, within the timescale of deglaciation.

While all the above mechanisms for barite genesis have attractive features to explain the occurrence of post-Marinoan deposits, they also carry distinct geochemical implications for Ba isotopes (summarized in Table 1). We test these geochemical predictions through a Ba isotopic survey of modern and paleo-environments and use these insights to discriminate between different models of post-Marinoan barite formation.

3. Materials and methods

3.1. Samples

A summary of all modern and Marinoan samples and sample-sites is provided in Fig. 1 and in the supplementary materials (Table S1). In Fig. 1, we plot sample locations of modern, and Proterozoic stratiform samples next to a reconstructed Marinoan paleogeographic map (Li et al., 2013) with locations of Marinoan-aged samples. To explore the isotopic expression of the modern Ba cycle in different depositional environments, we utilize an extensive collection of previously-described terrestrial, cold seep, hydrothermal, and core-top pelagic barites (Paytan et al., 1993, 1996; Paytan and Griffith, 2007; Griffith et al., 2018, and references therein; see supplementary materials Table S1). Modern core-top pelagic barite was separated from other mineral phases via a sequential extraction protocol outlined in Paytan et al. (1993). Proterozoic stratiform barites–which have been interpreted as forming under modern cold seep-like environments–are from the late Paleoproterozoic Cuddapah Supergroup (Mangampeta barites; Clark et al., 2004) and the Gams Formation in the Aggeneys-Gamsberg district of South Africa (McClung et al., 2007). The post-Marinoan (earliest Ediacaran; 635 Ma) barites used in this study were sampled from Minas Gerais State, Brazil (S 15°18′14.60″S, W 44°21′43.46″W), Northwest Territories, Canada (N 63°18.37′, W 127°09.76′), Finnmark, Norway (70°8′3.59″N, 28°15′11.46″E), and South China (N 31°41.74′, E 110°47.20′) (Fig. 1). Barite cements in each of these locations occur as 10–30 cm thick horizons within the post-glacial transgressive systems tract (TST) and occur along basement highs (for full site descriptions see Killingsworth et al., 2013; Crockford et al., 2016, 2018a). All samples were micro-drilled from polished surfaces and cut perpendicular to the radiating crystals (fans) from the cements. The drilled powders were then split for various isotopic analyses.

3.2. Analytical methods

All samples were prepared for Ba isotope analysis in the NIRVANA Laboratory clean rooms at Woods Hole Oceanographic Institution (WHOI) in class 100 laminar flow hoods using high-purity reagents (e.g., Ba-free Na_2CO_3) and acid-cleaned labware (e.g., PTFE, HDPE). For each sample, a ≈10 mg aliquot of barite was dissolved following a two-step process (cf. Horner et al., 2017 and references therein). First, barite was converted to witherite ($BaCO_3$) by reacting powders with a 1 M Na_2CO_3 solution at 90 °C for at least 18 h. This step was repeated three times to ensure complete conversion of $BaSO_4$ to $BaCO_3$; after the third reaction, the precipitate was rinsed with 18.2 MΩ H_2O to displace any residual Na_2CO_3 solution. Second, the witherite precipitate was dissolved using 2 M HCl. Aliquots of this solution were subsampled for multi-element and Ba-isotopic analyses.

Aliquots containing ≈100 ng of Ba were prepared for Ba-isotopic analysis. First, samples were spiked with a known quantity of a ^{135}Ba–^{136}Ba double spike (Bates et al., 2017; Horner et al., 2017) to achieve a spike- to sample-derived Ba concentration ratio of 1–2. These aliquots were equilibrated with the spike via addition of a few drops of concentrated HCl and drying—repeating this process at least two times—before being re-dissolved in 250 µL of 2 M HCl in preparation for ion-exchange chromatography. Barium was purified by passing samples gravimetrically through 500 µL of AG 50W-X8 (200–400 mesh) cation-exchange resin that was pre-cleaned of Ba with 6 M HCl. Matrix elements were eluted using 2 M HCl and Ba was eluted using 2 M HNO_3, which releases Ba from the resin while retaining rare earth elements that might interfere with Ba-isotopic analysis (Horner et al., 2015). All resin was discarded after a single use.

Purified aliquots of Ba were analyzed for their Ba-isotopic compositions using a Thermo Neptune multi-collector inductively coupled plasma mass spectrometer (ICP-MS) in low resolution mode at the WHOI Plasma Facility. Ion currents corresponding to m/z 131 (Xe), 135 (Ba), 136 (Xe, Ba, Ce), 137 (Ba), 138 (Ba, La, Ce), 139 (La), 140 (Ce) were simultaneously monitored in 30 × 4.19 s background-corrected integrations; all samples were analyzed in this manner at least four—and as many as eight—times. Sample isotopic compositions were calculated using a three-dimensional geometric interpretation of the double spike problem; calculations were performed iteratively in ^{138}Ba/^{135}Ba, ^{137}Ba/^{135}Ba, and ^{136}Ba/^{135}Ba space (the x-, y-, and z-axes, respectively) with additional nested loops for isobaric corrections (^{136}Xe and ^{136}Ce on ^{136}Ba; ^{138}Ce and ^{138}La on ^{138}Ba). Concentration- and spike-matched aliquots of NIST SRM 3104a were measured after every fourth sample, and sample Ba-isotopic compositions were calcu-

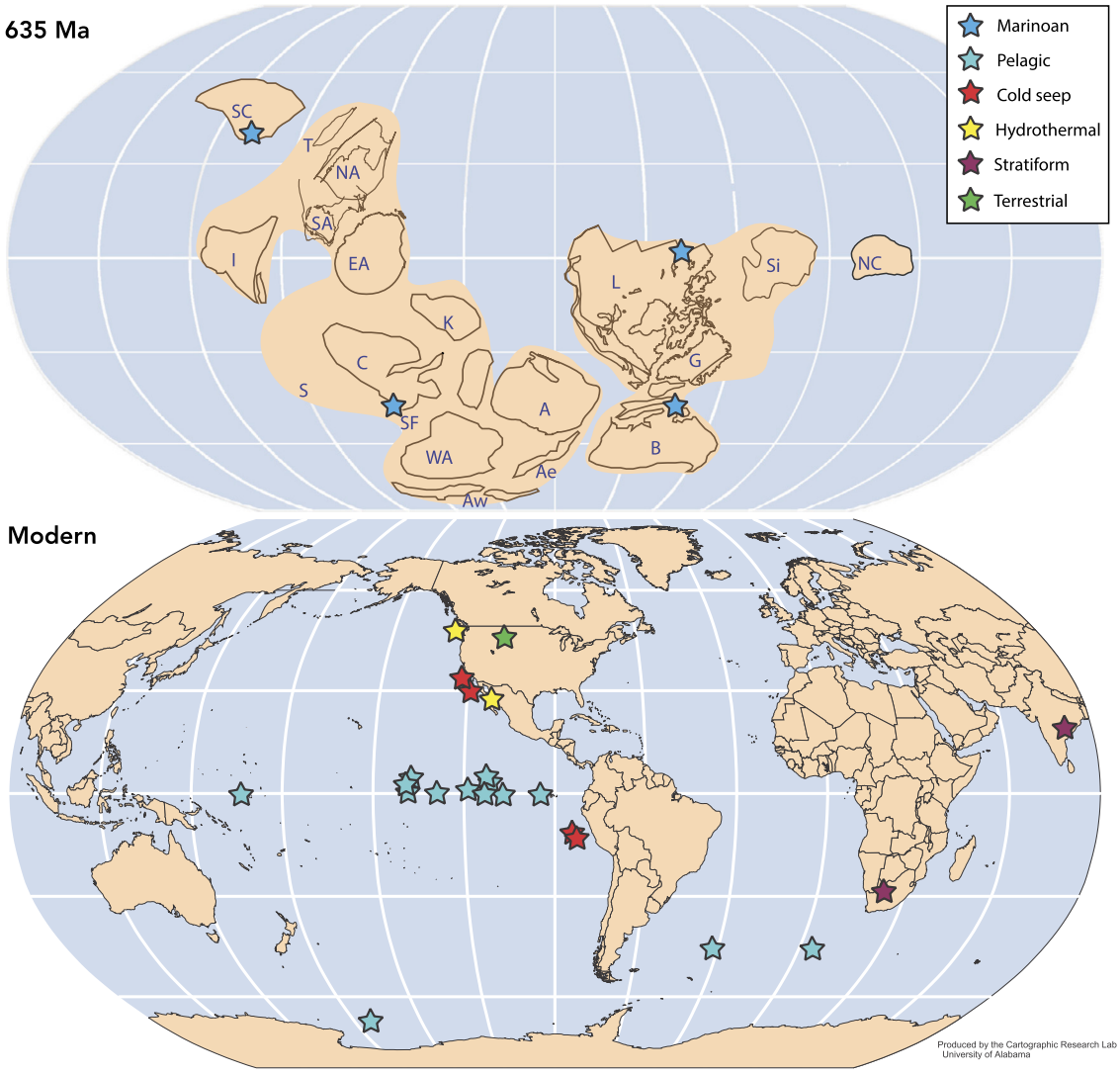

Fig. 1. Map of sample locations in modern and Marinoan aged samples. In the top panel a 635 Ma paleo-reconstruction map from Li et al. (2013) is presented with blue stars representing sampling locations. The lower panel depicts sampling locations of modern and Proterozoic stratiform barites.

lated relative to the moving average of the nearest four measurements of NIST SRM 3104a measurements (i.e., two behind, two ahead). A secondary standard, WHOI Ba Std (AccuSPEC), was analyzed in place of every 12th sample to monitor the accuracy of the time-dependent normalization to NIST SRM 3104a. All Ba-isotopic data were reported as deviations in the $^{138}Ba/^{134}Ba$ ratio relative to NIST SRM 3104a. All deviations are expressed in ‰:

$$\delta^{138/134}Ba_{NIST} = \left[\left(^{138}Ba/^{134}Ba\right)^{sample}/\left(^{138}Ba/^{134}Ba\right)^{NIST\ SRM\ 3104a} - 1\right]$$

Barium blanks resulting from barite dissolution and Ba purification were determined to be negligible, constituting no more than 0.1% of sample-derived Ba. These blanks were assessed by processing aliquots of double spike containing between 1–5 ng of Ba through the relevant procedures and calculating sample- (i.e., blank) derived Ba concentrations from isotopic dilution using the instrument mass-bias corrected $^{138}Ba/^{135}Ba$ ratio. Blanks from barite dissolution were determined as 50 and 125 pg Ba, and blanks from ion-exchange chromatography were assessed at 16 and 48 pg; all blanks were deemed insignificant and thus no blank corrections were made to either Ba concentration or isotopic data. Uncertainty, reported as two standard deviations about the mean (i.e., ±2 SD) for sample $\delta^{138/134}Ba_{NIST}$ is estimated as ±0.03‰ (Horner et al., 2015).

Lastly, five aliquots of NBS-127 (powdered barite standard from IAEA) were processed as unknowns and analyzed for their Ba-isotopic compositions over the course of this study. We report an unweighted mean $\delta^{138/134}Ba_{NIST}$ for NBS-127 of −0.29 ± 0.01‰ (±2 SD; $n = 3$), in agreement with values reported previously (e.g., −0.27 ± 0.02‰; $n = 3$, reported by Horner et al., 2017; −0.30 ± 0.02‰ by Bridgestock et al., pers. comm.).

3.3. Thermodynamic calculations of barite saturation

Thermodynamic simulations to calculate barite saturation under different Ba–SO_4 conditions were performed utilizing the PHREEQC computer code (Parkhurst and Appelo, 2013). Simulations were performed assuming a variable salinity (46–55), constant temperature (−3.5 °C), and constant pH (7.7) (Ashkenazy et al., 2013; Halevy and Bachan, 2017). The abundance of major dissolved species (Al, B, Br, C, Ca, Cl, F, K, Li, Mg, Na, Si and Sr) were scaled up to Marinoan salinities in proportion to their modern abundance ratios. A total of 169 simulations were performed for different combinations of [SO_4] and [Ba].

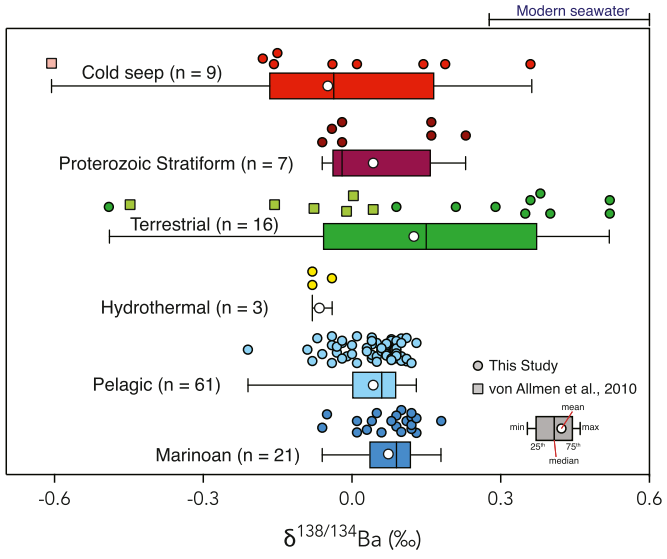

Fig. 2. Box and Whisker plots of $\delta^{138/134}Ba_{NIST}$ (x axis) results together with individual data points and population uncertainties. Results are separated by color and shape and are labeled along with the number of samples and separated along the y axis. Squares are previously published results from von Allmen et al. (2010) translated from $\delta^{137/134}Ba_{FLUKA}$ to $\delta^{138/134}Ba_{NIST}$ and circles represent new data from this study. The range of modern marine seawater $\delta^{138/134}Ba_{NIST}$ composition is presented in the top right corner of the figure. Black lines are median values, edges of colored boxes represent 25th and 75th quartiles, while whiskers represent the total data spread and white circles represent mean values. Uncertainty on individual $\delta^{138/134}Ba$ measurements (±2 SD) was typically less than ±0.03‰.

4. Results and discussion

4.1. Barium-isotopic survey of barites

The Ba-isotopic composition of modern barites combined with a handful of previously published results (von Allmen et al., 2010) shows systematic variations—in both mean $\delta^{138/134}Ba_{NIST}$ and magnitude of deviation about said mean—that correlate with the genetic origin of the deposit. It thus follows that the Ba-isotope composition (and variance) of samples of unknown genesis, such as the post-Marinoan barites, can be used as a diagnostic indicator of origin. Hydrothermal samples exhibit the lowest mean $\delta^{138/134}Ba_{NIST}$ value of -0.07 ± 0.02‰ ($n = 3$; Fig. 2). In contrast, modern marine pelagic barites have a mean $\delta^{138/134}Ba_{NIST}$ value of $+0.04 \pm 0.06$‰ ($n = 61$; Fig. 2). Modern cold seep samples have a mean composition that is more negative than modern pelagic barites and also have a significantly larger standard deviation ($n = 9$; $\delta^{138/134}Ba_{NIST} = -0.05 \pm 0.28$‰). These modern cold seep values show some similarity, both in median and variation—but not mean value—to suggested analogue Proterozoic stratiform barites ($n = 7$) from India and South Africa, with a $\delta^{138/134}Ba_{NIST}$ value of $+0.06 \pm 0.12$‰. Terrestrial samples are both more enriched in ^{138}Ba and much more variable than modern marine samples with a mean $\delta^{138/134}Ba_{NIST}$ value of $+0.12 \pm 0.31$‰ ($n = 16$; Fig. 2). Post-Marinoan barites display a relatively confined range of $\delta^{138/134}Ba_{NIST}$ values ($+0.08 \pm 0.06$‰; $n = 21$) that best overlaps with modern marine barites (Figs. 2 and 3). This survey of modern and ancient environments provides confidence for the use of Ba isotopes as an identifier of Ba source and, thus, depositional environment. Future development of Ba isotopes will prove fruitful in identifying depositional processes, particularly when combined

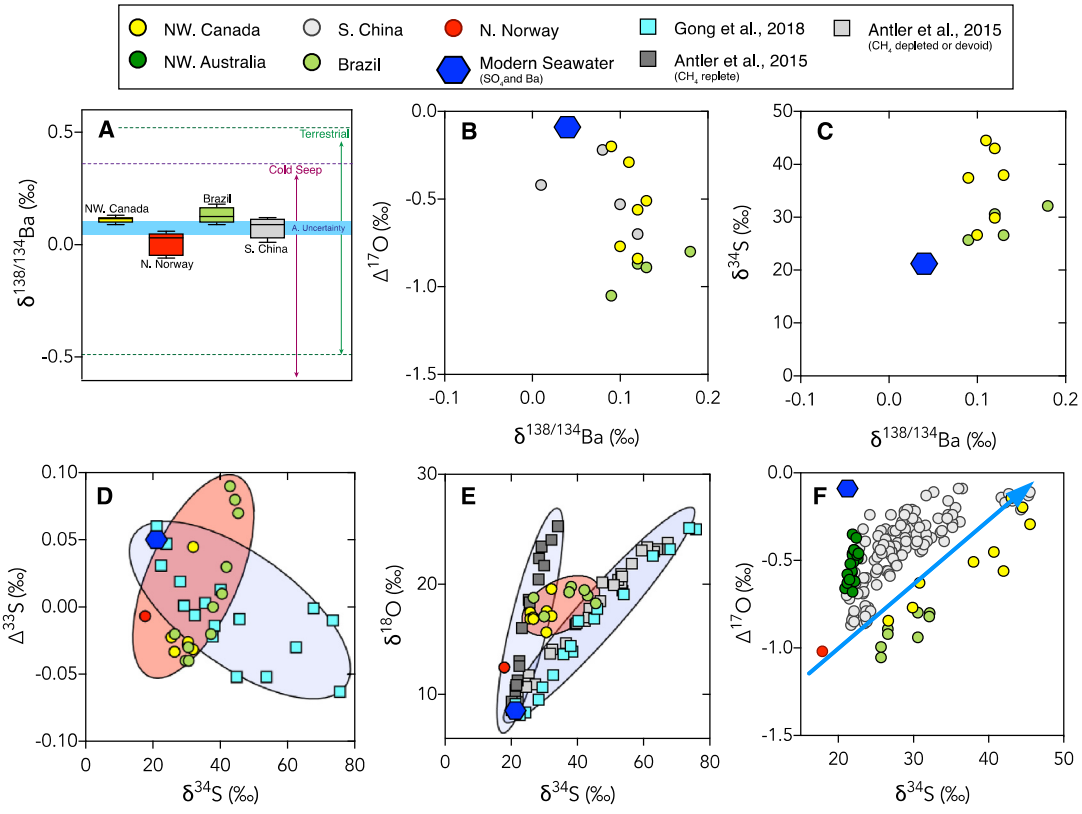

Fig. 3. (from left to right) A) Marinoan barite $\delta^{138/134}Ba$ data plotted for different sample locations along with associated uncertainties (±1 SD) on these, cold seep and terrestrial samples. The blue line represents the average (±2 SD) analytical uncertainty on individual measurements. B) $\Delta^{17}O$ vs. $\delta^{138/134}Ba$ are plotted. C) $\delta^{34}S$ vs. $\delta^{138/134}Ba$ values are plotted. D) $\Delta^{33}S$ vs. $\delta^{34}S$ values from Gong et al. (2018), Crockford et al. (2018a, 2019) are plotted. E) $\delta^{18}O$ vs. $\delta^{34}S$ values from Antler et al. (2015) and Crockford et al. (2018a) are plotted. F) $\Delta^{17}O$ vs. $\delta^{34}S$ values are plotted with the blue line with an arrow representing a suggested isotopic evolution of post-Marinoan SO_4 (Crockford et al., 2016, 2018a). Please refer to referenced publications for uncertainties on analyses.

with information from more established isotope systems (S, O, Ca, Sr e.g., Griffith et al., 2018).

4.2. Sources of SO_4 and Ba to post-Marinoan barites

4.2.1. Origin of sulfate

Barite from all Marinoan locations have yielded anomalous $\Delta^{17}O$ values ($\Delta^{17}O < -0.5‰$) and, in the case of Brazil, Northern Norway, Northwest Canada and South China (Peng et al., 2011; Killingsworth et al., 2013), correlate with sulfur isotopes as well (Crockford et al., 2016, 2018a; Fig. 3). These observations suggest synchronous post-Marinoan barite deposition. To synchronously precipitate appreciable amounts of barite, the syn-glacial Ba pool must have initially remained segregated from surface waters as SO_4 ingrowth occurred via continental weathering. Additional isotopic trends in post-Marinoan barites (i.e., $\delta^{18}O$–$\delta^{34}S$ and $\Delta^{33}S$–$\delta^{34}S$) significantly deviate from those of modern cold seep barites (Antler et al., 2015; Crockford et al., 2016; Gong et al., 2018). These observations suggest that post-Marinoan SO_4 was not isotopically imprinted by processes within a cold seep environment as SO_4 ingrowth occurred (Fig. 3), as has previously been suggested (Shields et al., 2007). These observations support a global surface SO_4 reservoir that was likely a unique transient scenario as a consequence of the Snowball state, where both high rates of post-glacial weathering would have made this global SO_4 reservoir highly modifiable by terrestrial runoff bearing the $\Delta^{17}O$ anomaly (Crockford et al., 2016), but also segregated from Ba-rich waters due to density driven stratification. Further supporting this stratified model is a lack of any coherent trends between SO_4 isotopes and coeval $\delta^{138/134}Ba_{NIST}$ data, suggesting that the SO_4-bearing reservoir evolved separately from that bearing Ba, and is consistent with the need for mixing at the interface of separate solutions enriched in either Ba or SO_4 (Fig. 3). These isotopic observations lend support for models that outline a long-lived freshwater lid that formed via rapid deglacial runoff and melting of sea ice (Shields, 2005; Liu et al., 2014; Yang et al., 2017) that has been colloquially named 'Glacial Lake Harland' (Hoffman et al., 2017).

4.2.2. Origin of barium

In comparing Ba isotopic values of post-Marinoan barites to modern samples, only modern pelagic samples exhibit a similar mean $\delta^{138/134}Ba_{NIST}$ value (Fig. 2). We interpret this isotopic similarity as implying that post-Marinoan barites likely formed under a marine scenario, but due to differences in sample set sizes between barite type and overlap in $\delta^{138/134}Ba_{NIST}$ values (Fig. 2) we explore alternative scenarios. Barites from terrestrial settings exhibit different mean $\delta^{138/134}Ba_{NIST}$ and larger variations than post-Marinoan samples. Thus, if post-Marinoan barites were derived from terrestrial sources we might expect to see greater Ba isotopic variability within individual deposits, and locality-specific mean values (Fig. 2). Accordingly, we rule out a riverine- or subterranean groundwater discharge-mediated Ba source to post-Marinoan barites.

Though cold seep deposits overlap in $\delta^{138/134}Ba_{NIST}$ values with post-Marinoan barites, the wide range in $\delta^{138/134}Ba_{NIST}$ values ($\pm 0.28‰$) is incompatible with the narrow spread exhibited by post-Marinoan barites ($\pm 0.06‰$; modern marine barites possess a similarly narrow range of $\pm 0.06‰$). While we acknowledge that the cold seep sample size is relatively small ($n = 9$)—warranting additional studies of Ba in seep environments—we can draw on four additional lines of evidence in considering whether post-Marinoan barites were deposited in seep-like environments. First, the Ba isotope variation exhibited by Proterozoic stratiform barites (interpreted as possible analogues to modern seep samples), also bears a large variability in $\delta^{138/134}Ba_{NIST}$ values like modern seeps, supporting a common genetic origin (Fig. 2). Second, though SO_4 isotope data imply a single SO_4 reservoir (from $\Delta^{17}O$–$\delta^{34}S$ data), this reservoir did not develop through anaerobic-oxidation of CH_4 (from $\Delta^{33}S$–$\delta^{34}S$ and $\delta^{34}S$–$\delta^{18}O$ trends). Thus, these data are also incompatible with a seep-like origin for post-Marinoan barites (Fig. 3). Third, field observations show that post-Marinoan barite horizons often outcrop along basement and/or topographic highs with very thin or even no underlying cap dolostones (e.g., Brazil and Norway; Crockford et al., 2018a). Thus, a sedimentary Ba origin would require the unlikely scenario whereby diverse, geographically-disparate strata synchronously supply isotopically-similar Ba toward the locations of barite precipitation. Fourth, morphological characteristics of post-Marinoan barites, with fanning and digitate textures that indicate prolonged growth into solution (Hoffman et al., 2011), are not observed in modern seep environments. Thus, we interpret the global and synchronous deposition of isotopically and morphologically similar post-Marinoan barites as pointing towards a single, large, homogeneous Ba source.

Based on the Ba-isotopic similarity between modern marine and Marinoan barites, we contend that this source was seawater. Emerging datasets for seawater (e.g., Bates et al., 2017; Hsieh and Henderson, 2017), sediments (Bridgestock et al., 2018, 2019), and particulates (Horner et al., 2017) imply a fractionation of between -0.4 and $-0.5‰$ during barite precipitation from seawater. Thus, the absolute value of post-Marinoan barite $\delta^{138/134}Ba_{NIST}$ requires a contemporary seawater value to have been between $+0.5$ and $+0.6‰$, similar to modern surface seawater (e.g., Horner et al., 2015). Although the post-Marinoan ocean was likely much different from the modern ocean, a marine reservoir characterized by $\delta^{138/134}Ba_{NIST} \approx +0.5‰$ is perfectly plausible if barite constituted the major sink of Ba from the ocean during the Marinoan, as it does today.

In the modern ocean, dissolved Ba is ultimately sourced from the weathering of silicates and delivered to the ocean via terrestrial riverine runoff and subterranean groundwater discharge, along with a small hydrothermal flux (Dickens et al., 2003). Though there is considerable variability between local sources on aggregate (Cao et al., 2016), the average input $\delta^{138/134}Ba_{NIST}$ value is $\approx +0.1‰$ (Nan et al., 2018). Dissolved Ba is then stripped from surface waters through biologically-mediated precipitation of pelagic barite with a fractionation of $\approx -0.5‰$, even though modern marine Ω_{barite} is slightly below unity. This pelagic removal flux balances both the isotopic composition (mean pelagic barite $\delta^{138/134}Ba_{NIST} = +0.04 \pm 0.06‰$) and flux of Ba to seawater, resulting in a Ba residence time of $\approx 10^4$ years (e.g., Dickens et al., 2003). During a Snowball Earth, however, the residence time of Ba was likely far longer on account of the lower SO_4 concentrations within—and terrestrial SO_4 fluxes to—the syn-glacial ocean. Accordingly, the Ba concentration at which Ω_{barite} approached unity would likely be far higher than today, as is the case in modern SO_4 poor semi-restricted basins (e.g., Falkner et al., 1993; Fig. 4). Despite diminished terrestrial fluxes, low marine Ω_{barite} would have facilitated a significant Ba inventory to accumulate from hydrothermal sources or perhaps seafloor weathering until Ba concentrations reached a level where Ω_{barite} approached unity and barite precipitation resumed (Fig. 4). This precipitation could have been mediated by organic matter degradation or hydrothermal circulation (e.g., Tivey, 2007). Organic matter could have been supplied to seawater from both moulin flushes—sourced from a fledgling surface biosphere that grew in cryoconite pans on surface ice (Hoffman, 2016)—as well as by export production from productive waters between cracks in sea ice. Regardless, so long as some form of barite precipitation occurred, a well-mixed (Ashkenazy et al., 2013), large Ba pool, characterized by values $+0.5‰$ heavier than average inputs would have developed (Figs. 2 and 3). If this deep marine reservoir was the sole Ba source to post-Marinoan barites, the re-

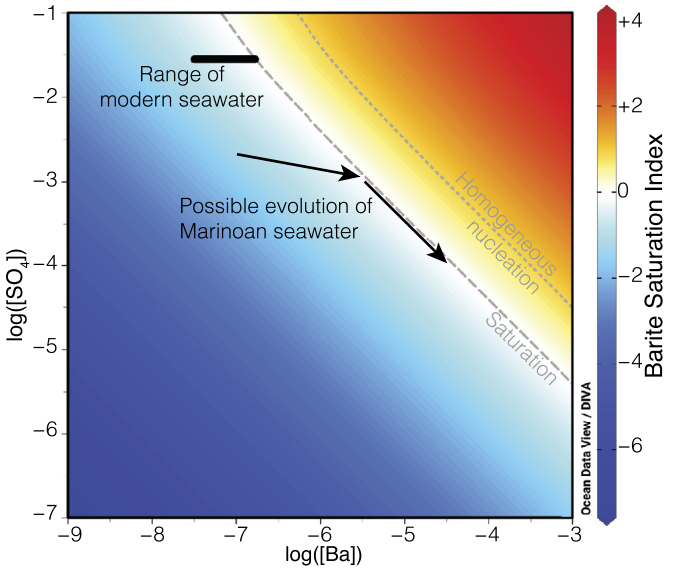

Fig. 4. Barite saturation index as a function of log([SO_4]) and log([Ba]) in the syn-glacial Marinoan ocean plotted as moles/L (M). Results are interpolated across the property space using Ocean Data View (Schlitzer, 2011). Dashed and dotted lines correspond to saturation ($\Omega_{barite} = 1$) and homogeneous nucleation ($\Omega_{barite} = 8$) respectively. Since the Ba-isotopic composition of post-Marinoan barites implies a marine Ba source in equilibrium with barite, the syn-glacial Marinoan ocean must have initially approached and subsequently fallen along the dashed line marked 'saturation'. The shallow slope of the arrow approaching the saturation line (indicating greater SO_4 relative to Ba removal) is a function of additional sinks for SO_4 beyond $BaSO_4$ precipitation such as hydrothermal SO_4 reduction, and dissimilatory SO_4 reduction. Note that the ranges corresponding to modern seawater are purely illustrative, as the underlying saturation field for present-day seawater is shifted on account of the lower salinities and higher temperatures and pH compared to the Marinoan.

sultant precipitates would exhibit a narrow compositional range similar to that of the inputs (≈+0.1‰; Nan et al., 2018). As such, we consider both the absolute composition (+0.08‰) and narrow range (±0.06‰) of post-Marinoan barites as strong evidence of a well-mixed, effectively limitless marine source characterized by $\delta^{138/134}Ba_{NIST}$ between +0.5 and +0.6‰ (Figs. 2 and 3). While precise Ba concentrations are difficult to infer for the subglacial Marinoan ocean, they were likely much higher than the modern ocean on account of the increased salinity (Ashkenazy et al., 2013) and low ambient SO_4 concentration (Fig. 4). Such geologically-unusual conditions may have promoted unprecedented high Ba concentrations accounting for the thus far singular occurrence of this type of barite deposit in the geological record.

4.3. Geological significance of post-Marinoan barites

In addition to considering the fluid sources of Ba and SO_4 to post-Marinoan barites, it is worthwhile to consider the geological mechanisms by which these deposits formed and why there are no equivalent deposits marking the terminus of other Snowball Earth events. We discuss both issues below.

4.3.1. Genesis of post-Marinoan barites

In a stratified ocean, a salty (salinity ≈50 ppt; Ashkenazy et al., 2013), high-Ba (but low-SO_4) subglacial pool would have built up during the glaciation (Fig. 4). Upon deglaciation, a resumption of continental weathering would have supplied SO_4 into meltwaters that would have capped the post-glacial ocean. Elevated post-glacial primary productivity (Kunzmann et al., 2013) would have likely kept surface water Ba concentrations low due to the reestablishment of a biological pump to deep waters. Warming of fresh surface waters would have maintained a stratified ocean, segregating Ba-rich deep water from relatively SO_4-rich surface waters for an estimated 10^4 years after the Marinoan glaciation (Liu et al., 2014; Crockford et al., 2016; Yang et al., 2017). In certain locations where deposition of other sediment-types was extremely limited (i.e., local topographic highs) the interface between the syn-glacial Ba reservoir and SO_4-rich surface layer would be primed to precipitate barite with distinct Ba and SO_4 isotopic signals.

We consider three possibilities to account for the occurrence of barite precipitates within the Marinoan post-glacial TST. First, Ba-rich waters may have upwelled to meet SO_4-rich surface waters after cap dolostone deposition, which would have resulted in the formation of seafloor barite cements where this mixing occurred near the seabed. Second, Ba may have been initially incorporated into primary carbonate phases and then expelled during early dolomitization of the original calcite or aragonite in the underlying cap carbonates. Under such a scenario, cap carbonates would have had to precipitate out of seawater (to record marine $\delta^{138/134}Ba_{NIST}$ values), which contrasts with suggestions that these units precipitated in freshwater (Shields, 2005) as aragonite with an isotopic composition that was significantly offset from glacial seawater. A third possibility is that Ba was brought in with seawater through advective transport (also sourcing Mg) during fluid buffered early dolomitization of primary carbonate phases and incorporated into barite that precipitated at the interface between the meltwater surface layer (supplying SO_4) and seawater (supplying Ba; Ahm et al., 2019). This third possibility, while supported by recent studies documenting significant Ba enrichments in some carbonate phases within cap dolostones of Brazil (Okubo et al., 2018) and South Australia (Hood and Wallace, 2015) as well as being consistent with a limited range in $\delta^{138/134}Ba_{NIST}$ values of post-Marinoan barites, is in conflict with other locations in Australia that contain $\Delta^{17}O$ anomalies in carbonate-associated SO_4 within cap dolostones (Bao et al., 2012). Moreover, in Norway and Brazil, barites occur above highly condensed cap dolostone sections or directly on crystalline basement (Crockford et al., 2018a), obviating the need for extensive dolomitization of underlying units. Thus, the first explanation is the only model that satisfies all geochemical and field observations from all localities, though we cannot yet rule out whether the Ba-rich waters were sourced by advective flow of Ba sourced from dolomitization of proximal or possibly distal cap carbonates.

Models that source Ba from a marine reservoir also explain why barite deposition, in some locations, takes place above cap dolostones and not below them, as it marks the transition between underlying dolostones and overlying limestones. At this time, and preceding a breakdown in stratification, $\Delta^{17}O$ anomalies would have had time to build up within the freshwater surface ocean that would have effectively comprised the global marine SO_4 reservoir (Crockford et al., 2016). Although it is difficult to rule out transient barite precipitation and rapid subsequent quantitative dissolution in certain locations via a migrating freshwater-seawater interface, it appears that environmental factors converged synchronously across globally disparate margins to preserve these unique horizons. This model further highlights that post-Marinoan barite horizons represent a spatially specific and very unique convergence of events: SO_4-rich surface waters bearing anomalous $\Delta^{17}O$ values were able to interact (and precipitate barite from) Ba-rich seawater until the breakdown of post-glacial stratification. The geological precision of this model allows us to explore why globally synchronous barite precipitation appears to be unique to the Marinoan glaciation.

4.3.2. Speculations on the temporal expression of cryogenian barite

The preceding discussion outlines an internally consistent, holistic geochemical and geological framework for generating barite horizons in the aftermath of a Snowball Earth glaciation. Given this—or any other—barite formation mechanism, the uniqueness of post-glacial barite horizons to post-Marinoan-aged strata

remains a challenge to explain. In our suggested model of barite precipitation, a syn-glacial Ba-rich and SO_4-poor marine reservoir builds up during the Marinoan Snowball Earth event. Once CO_2 buildup triggers deglaciation, terrestrial weathering resumes and new SO_4 from pyrite oxidation spreads across global marine surface waters. At the interface between these reservoirs, barite precipitation occurs until stratification breaks down and ocean waters return to a barite-undersaturated preglacial state. Considering that the key differences between the Sturtian and Marinoan 'events' is their duration (≈3–15.2 Myrs versus 57–59 Myrs, respectively; Hoffman et al., 2017 and references therein) and relative sequence (Sturtian preceded Marinoan), why then might glacially-associated barite horizons only be observed in post-Marinoan strata?

We put forth two possible mechanisms that may account for the lack of post-Sturtian barite: these horizons are either 'missing' (i.e., lack of preservation) or are absent entirely (i.e., lack of accumulation). In the first case, a longer Sturtian glaciation potentially allowed for greater subsidence along continental margins. Assuming that barite preservation is partially incumbent upon being cased within or below cap carbonate sequences, greater subsidence would have ultimately moved the locations of barite and cap carbonate deposition apart from one another by shifting the locus of TST deposition further inland, making cap carbonate preservation far less favorable (Hoffman et al., 2017). While TSTs may have been shifted inland, greater subsidence along continental margins may have forced the interface between SO_4-rich surface waters and Ba-rich seawater deeper for the Sturtian versus the Marinoan, therefore limiting preservation potential. This model is consistent with the overall rarity of Sturtian-aged TSTs. Alternatively, a larger contribution of carbonate weathering for the Marinoan deglaciation (due to weathering post-Sturtian carbonates), may have delayed oversaturation and subsequent cap carbonate deposition within Sturtian waters, which, in turn, reduced the potential for barite preservation within or below cap carbonate sequences.

Deposition and/or preservation of post-glacial barites in the Sturtian may also relate to the dynamics of the oxygen cycle. A longer Sturtian glacial interval may have allowed for a larger atmospheric O_2 reservoir to build up across the Sturtian than the Marinoan due to prolonged O_2 export from primary production beneath cracks in ice or within cryoconite pans, but, at the same time, with limited O_2 sinks due to greatly diminished oxidative weathering (Hoffman, 2016; Laakso and Schrag, 2017). During deglaciation, this high-O_2 state may have translated into a Sturtian marine oxidant reservoir that was larger than that in the Marinoan. If this oxidative deepening outpaced the growth of the post-Sturtian freshwater lens, the source of Ba to SO_4-rich surface waters might have been limited. Alternatively, a deeper oxic-anoxic chemocline may have only allowed the surface ocean to adopt a modern-like Ba-cycle dominated by barite precipitation in organic-rich microenvironments. In this case, barite may have only accumulated as microcrystals in post-Sturtian shales sourced through export production, rather than as the thick horizons found in Marinoan cap carbonates. That is, if only a pelagic Ba cycle was resumed in the immediate aftermath of the Sturtian glaciation, possibly because of a deeper oxic-anoxic chemocline or a shorter-lived post-glacial stratification, the conditions necessary to achieve barite supersaturation at the freshwater–seawater interface may never have been met and thus no significant barite horizons formed. The discovery of microcrystalline barite with non-zero $\Delta^{17}O$ values would lend support to this hypothesis.

Although the above scenarios are certainly plausible, we concede that the absence of evidence does not constitute strong evidence of absence, particularly when relying on a sparse sedimentary record. It is important to note, that of the 48 documented post-Marinoan sequences (Hoffman et al., 2017), only seven have documented barite occurrences, and even in such cases, the footprint of barites is only exposed in a small minority of locations within the broader areas housing post-Marinoan sequences. Therefore, one cannot rule out the possibility that post-Sturtian barites exist in a subset of the 39 locations that have exposed post-Sturtian strata (Hoffman et al., 2017), but they have yet to be discovered.

5. Conclusions

Barium-isotopic insights are rapidly improving our understanding of the modern and ancient Ba cycle and thus illuminating the genetic origin of ancient barites. Here, we applied this emerging tool to enigmatic post-Marinoan barite horizons to explore their formation mechanism. Augmented by a Ba-isotopic survey of barites from diverse modern environments, we contend that the Ba source to the post-Marinoan deposits was an effectively limitless, well-mixed, subglacial seawater reservoir. Barite horizons were subsequently deposited at the nexus of this Ba-rich reservoir and that of a relatively SO_4-rich meltwater surface layer during the deglaciation. This precipitation occurred globally, synchronously, and from an isotopically-homogeneous Ba source until the breakdown of post-glacial stratification, which likely shifted the Ba cycle toward a more modern-like state. In addition to demonstrating the utility of Ba isotopes to interrogate the genesis of barite deposits, our study does not preclude the possibility that analogous barite horizons or $\Delta^{17}O$-anomaly-bearing disseminated barites were formed in the aftermath of other major Snowball Earth-like glaciations, therefore, continued exploration for them is strongly encouraged.

Acknowledgements

The authors thank: Dalton Hardisty and Bryan Killingsworth for insightful reviews that improved this manuscript; Lou Derry for editorial handling and constructive comments; Paul F. Hoffman for NW Canada samples and engaging discussions; Maureen Auro for laboratory assistance; Harry McClelland for comments on an early version of this manuscript; and the Halevy Group at the Weizmann Institute of Science for insightful discussions. This research was made possible with support from the University of Colorado Boulder, the Agouron Institute, and the Geological Society of America (PWC); Natural Sciences and Engineering Research Council (MSWH); Carlsberg Foundation (ASCA); Conselho Nacional de Pesquisa Científica and Fundação de Amparo à Pesquisa do Estado de Minas Gerais (FC and GU); and the U.S. National Science Foundation (TJH and AP).

Appendix A. Supplementary material

Supplementary material related to this article can be found online at https://doi.org/10.1016/j.epsl.2019.05.018.

References

Ahm, A.S.C., Maloof, A.C., Macdonald, F.A., Hoffman, P.F., Bjerrum, C.J., Bold, U., Rose, C.V., Strauss, J.V., Higgins, J.A., 2019. An early diagenetic deglacial origin for basal Ediacaran "cap dolostones". Earth Planet. Sci. Lett. 506, 292–307. https://doi.org/10.1016/j.epsl.2018.10.046.

Antler, G., Turchyn, A.V., Herut, B., Sivan, O., 2015. A unique isotopic fingerprint of sulfate-driven anaerobic oxidation of methane. Geology 43 (7), 619–622. https://doi.org/10.1130/G36688.1.

Ashkenazy, Y., Gildor, H., Losch, M., Macdonald, F.A., Schrag, D.P., Tziperman, E., 2013. Dynamics of a Snowball Earth ocean. Nature 495 (7439), 90. https://doi.org/10.1038/nature11894.

Bao, H., Lyons, J.R., Zhou, C., 2008. Triple oxygen isotope evidence for elevated CO_2 levels after a Neoproterozoic glaciation. Nature 453 (7194), 504. https://doi.org/10.1038/nature06959.

Bao, H., Chen, Z.Q., Zhou, C., 2012. An ^{17}O record of late Neoproterozoic glaciation in the Kimberley region, Western Australia. Precambrian Res. 216, 152–161. https://doi.org/10.1016/j.precamres.2012.06.019.

Bates, S.L., Hendry, K.R., Pryer, H.V., Kinsley, C.W., Pyle, K.M., Woodward, E.M.S., Horner, T.J., 2017. Barium isotopes reveal role of ocean circulation on barium cycling in the Atlantic. Geochim. Cosmochim. Acta 204, 286–299. https://doi.org/10.1016/j.gca.2017.01.043.

Bender, M., Sowers, T., Labeyrie, L., 1994. The Dole effect and its variations during the last 130,000 years as measured in the Vostok ice core. Glob. Biogeochem. Cycles 8 (3), 363–376.

Bitterwolf, K.K., Horner, T.J., Auro, M., Peucker-Ehrenbrink, B., Paytan, A., 2017. The barium isotopic composition of the global groundwater flux. In: Goldschmidt Abstracts, 356.

Bridgestock, L., Hsieh, Y.T., Porcelli, D., Homoky, W.B., Bryan, A., Henderson, G.M., 2018. Controls on the barium isotope compositions of marine sediments. Earth Planet. Sci. Lett. 481, 101–110. https://doi.org/10.1016/j.epsl.2017.10.019.

Bridgestock, L., Hsieh, Y.T., Porcelli, D., Henderson, G.M., 2019. Increased export production during recovery from the Paleocene–Eocene thermal maximum constrained by sedimentary Ba isotopes. Earth Planet. Sci. Lett. 510, 53–63. https://doi.org/10.1016/j.epsl.2018.12.036.

Cao, X., Bao, H., 2013. Dynamic model constraints on oxygen-17 depletion in atmospheric O_2 after a snowball Earth. Proc. Natl. Acad. Sci. USA 110 (36), 14546–14550. https://doi.org/10.1073/pnas.1302972110.

Cao, Z., Siebert, C., Hathorne, E.C., Dai, M., Frank, M., 2016. Constraining the oceanic barium cycle with stable barium isotopes. Earth Planet. Sci. Lett. 434, 1–9. https://doi.org/10.1016/j.epsl.2015.11.017.

Charette, M.A., Sholkovitz, E.R., Hansel, C.M., 2005. Trace element cycling in a subterranean estuary: Part 1. Geochemistry of the permeable sediments. Geochim. Cosmochim. Acta 69 (8), 2095–2109. https://doi.org/10.1016/j.gca.2004.10.024.

Chow, T.J., Goldberg, E.D., 1960. On the marine geochemistry of barium. Geochim. Cosmochim. Acta 20 (3–4), 192–198.

Clark, S.H., Poole, F.G., Wang, Z., 2004. Comparison of some sediment-hosted, stratiform barite deposits in China, the United States and India. Ore Geol. Rev. 24 (1–2), 85–101. https://doi.org/10.1016/j.oregeorev.2003.08.009.

Crockford, P.W., Cowie, B.R., Johnston, D.T., Hoffman, P.F., Sugiyama, I., Pellerin, A., Bui, T.H., Hayles, J., Halverson, G.P., Macdonald, F.A., Wing, B.A., 2016. Triple oxygen and multiple sulfur isotope constraints on the evolution of the post-Marinoan sulfur cycle. Earth Planet. Sci. Lett. 435, 74–83. https://doi.org/10.1016/j.epsl.2015.12.017.

Crockford, P.W., Hodgskiss, M.S., Uhlein, G.J., Caxito, F., Hayles, J.A., Halverson, G.P., 2018a. Linking paleocontinents through triple oxygen isotope anomalies. Geology 46 (2), 179–182. https://doi.org/10.1130/G39470.1.

Crockford, P.W., Hayles, J.A., Bao, H., Planavsky, N.J., Bekker, A., Fralick, P.W., Halverson, G.P., Bui, T.H., Peng, Y., Wing, B.A., 2018b. Triple oxygen isotope evidence for limited mid-Proterozoic primary productivity. Nature 559 (7715), 613. https://doi.org/10.1038/s41586-018-0349-y.

Crockford, P.W., Kunzmann, M., Bekker, A., Hayles, J., Bao, H., Halverson, G.P., Peng, Y., Bui, T.H., Cox, G.M., Gibson, T.M., Wörndle, S., 2019. Claypool continued: extending the isotopic record of sedimentary sulfate. Chem. Geol. 513, 200–225. https://doi.org/10.1016/j.chemgeo.2019.02.030.

Dickens, G.R., Fewless, T., Thomas, E., Bralower, T.J., 2003. Excess barite accumulation during the Paleocene-Eocene Thermal Maximum: massive input of dissolved barium from seafloor gas hydrate reservoirs. Spec. Pap., Geol. Soc. Am., 11–24.

Falkner, K.K., Bowers, T.S., Todd, J.F., Lewis, B.L., Landing, W.M., Edmond, J.M., 1993. The behavior of barium in anoxic marine waters. Geochim. Cosmochim. Acta 57 (3), 537–554. https://doi.org/10.1016/0016-7037(93)90366-5.

Gong, S., Peng, Y., Bao, H., Feng, D., Cao, X., Crockford, P.W., Chen, D., 2018. Triple sulfur isotope relationships during sulfate-driven anaerobic oxidation of methane. Earth Planet. Sci. Lett. 504, 13–20. https://doi.org/10.1016/j.epsl.2018.09.036.

Gonneea, M.E., Mulligan, A.E., Charette, M.A., 2013. Seasonal cycles in radium and barium within a subterranean estuary: implications for groundwater derived chemical fluxes to surface waters. Geochim. Cosmochim. Acta 119, 164–177. https://doi.org/10.1016/j.gca.2013.05.034.

Griffith, E.M., Paytan, A., Wortmann, U.G., Eisenhauer, A., Scher, H.D., 2018. Combining metal and nonmetal isotopic measurements in barite to identify mode of formation. Chem. Geol. 500, 148–158. https://doi.org/10.1016/j.chemgeo.2018.09.031.

Halevy, I., Bachan, A., 2017. The geologic history of seawater pH. Science 355 (6329), 1069–1071.

Hoffman, P.F., Macdonald, F.A., Halverson, G.P., 2011. Chemical sediments associated with Neoproterozoic glaciation: iron formation, cap carbonate, barite and phosphorite. Mem. Geol. Soc. Lond. 36 (1), 67–80. https://doi.org/10.1144/M36.5.

Hoffman, P.F., 2016. Cryoconite pans on Snowball Earth: supraglacial oases for Cryogenian eukaryotes? Geobiology 14 (6), 531–542. https://doi.org/10.1111/gbi.12191.

Hoffman, P.F., Abbot, D.S., Ashkenazy, Y., Benn, D.I., Brocks, J.J., Cohen, P.A., Cox, G.M., Creveling, J.R., Donnadieu, Y., Erwin, D.H., Fairchild, I.J., 2017. Snowball Earth climate dynamics and Cryogenian geology-geobiology. Sci. Adv. 3 (11), e1600983. https://doi.org/10.1126/sciadv.1600983.

van Smeerdijk Hood, A., Wallace, M.W., 2015. Extreme ocean anoxia during the Late Cryogenian recorded in reefal carbonates of Southern Australia. Precambrian Res. 261, 96–111. https://doi.org/10.1016/j.precamres.2015.02.008.

Horner, T.J., Kinsley, C.W., Nielsen, S.G., 2015. Barium-isotopic fractionation in seawater mediated by barite cycling and oceanic circulation. Earth Planet. Sci. Lett. 430, 511–522. https://doi.org/10.1016/j.epsl.2015.07.027.

Horner, T.J., Pryer, H.V., Nielsen, S.G., Crockford, P.W., Gauglitz, J.M., Wing, B.A., Ricketts, R.D., 2017. Pelagic barite precipitation at micromolar ambient sulfate. Nat. Commun. 8 (1), 1342. https://doi.org/10.1038/s41467-017-01229-5.

Hsieh, Y.T., Henderson, G.M., 2017. Barium stable isotopes in the global ocean: tracer of Ba inputs and utilization. Earth Planet. Sci. Lett. 473, 269–278. https://doi.org/10.1016/j.epsl.2017.06.024.

Hurtgen, M.T., Halverson, G.P., Arthur, M.A., Hoffman, P.F., 2006. Sulfur cycling in the aftermath of a 635-Ma snowball glaciation: evidence for a syn-glacial sulfidic deep ocean. Earth Planet. Sci. Lett. 245 (3–4), 551–570. https://doi.org/10.1016/j.epsl.2006.03.026.

Killingsworth, B.A., Hayles, J.A., Zhou, C., Bao, H., 2013. Sedimentary constraints on the duration of the Marinoan Oxygen-17 Depletion (MOSD) event. Proc. Natl. Acad. Sci. USA 110 (44), 17686–17690. https://doi.org/10.1073/pnas.1213154110.

Kirschvink, J.L., 1992. Late Proterozoic low-latitude global glaciation: the snowball Earth. In: The Proterozoic Biosphere: A Multidisciplinary Study. Cambridge University Press, New York. ISBN 9780521366151, pp. 51–52.

Kunzmann, M., Halverson, G.P., Sossi, P.A., Raub, T.D., Payne, J.L., Kirby, J., 2013. Zn isotope evidence for immediate resumption of primary productivity after snowball Earth. Geology 41 (1), 27–30. https://doi.org/10.1130/G33422.1.

Laakso, Thomas Andrew, Schrag, D.P., 2017. A theory of atmospheric oxygen. Geobiology 15 (3), 366–384. https://doi.org/10.1111/gbi.12230.

Li, Z.X., Evans, D.A., Halverson, G.P., 2013. Neoproterozoic glaciations in a revised global palaeogeography from the breakup of Rodinia to the assembly of Gondwanaland. Sediment. Geol. 294, 219–232. https://doi.org/10.1016/j.sedgeo.2013.05.016.

Liu, C., Wang, Z., Raub, T.D., Macdonald, F.A., Evans, D.A., 2014. Neoproterozoic cap dolostone deposition in stratified glacial meltwater plume. Earth Planet. Sci. Lett. 404, 22–32.

Luz, B., Barkan, E., Bender, M.L., Thiemens, M.H., Boering, K.A., 1999. Triple-isotope composition of atmospheric oxygen as a tracer of biosphere productivity. Nature 400 (6744), 547.

Martinez-Ruiz, F., Paytan, A., Gonzalez-Muñoz, M.T., Jroundi, F., Abad, M.M., Lam, P.J., Bishop, J.K.B., Horner, T.J., Morton, P.L., Kastner, M., 2019. Barite formation in the ocean: origin of amorphous and crystalline precipitates. Chem. Geol. 511, 441–451. https://doi.org/10.1016/j.chemgeo.2018.09.011.

McClung, C.R., Gutzmer, J., Beukes, N.J., Mezger, K., Strauss, H., Gertloff, E., 2007. Geochemistry of bedded barite of the Mesoproterozoic Aggeneys-Gamsberg Broken hill-type district, South Africa. Miner. Depos. 42 (5), 537–549. https://doi.org/10.1007/s00126-007-0128-4.

Nan, X.Y., Yu, H.M., Rudnick, R.L., Gaschnig, R.M., Xu, J., Li, W.Y., Zhang, Q., Jin, Z.D., Li, X.H., Huang, F., 2018. Barium isotopic composition of the upper continental crust. Geochim. Cosmochim. Acta 233, 33–49. https://doi.org/10.1016/j.gca.2018.05.004.

Okubo, J., Muscente, A.D., Luvizotto, G.L., Uhlein, G.J., Warren, L.V., 2018. Phosphogenesis, aragonite fan formation and seafloor environments following the Marinoan glaciation. Precambrian Res. 311, 24–36. https://doi.org/10.1016/j.precamres.2018.04.002.

Pack, A., Höweling, A., Hezel, D.C., Stefanak, M.T., Beck, A.K., Peters, S.T., Folco, L., 2017. Tracing the oxygen isotope composition of the upper Earth's atmosphere using cosmic spherules. Nat. Commun. 8, 15702. https://doi.org/10.1038/ncomms15702.

Parkhurst, D.L., Appelo, C.A.J., 2013. Description of Input and Examples for PHREEQC Version 3: A Computer Program for Speciation, Batch-Reaction, One-Dimensional Transport, and Inverse Geochemical Calculations (No. 6-A43). US Geological Survey.

Paytan, A., Kastner, M., Martin, E.E., Macdougall, J.D., Herbert, T., 1993. Marine barite as a monitor of seawater strontium isotope composition. Nature 366 (6454), 445. https://doi.org/10.1038/366445a0.

Paytan, A., Kastner, M., Chavez, F.P., 1996. Glacial to interglacial fluctuations in productivity in the equatorial Pacific as indicated by marine barite. Science 274 (5291), 1355–1357. https://doi.org/10.1126/science.274.5291.1355.

Paytan, A., Griffith, E.M., 2007. Marine barite: recorder of variations in ocean export productivity. Deep-Sea Res., Part 2, Top. Stud. Oceanogr. 54 (5–7), 687–705. https://doi.org/10.1016/j.dsr2.2007.01.007.

Peng, Y., Bao, H., Zhou, C., Yuan, X., 2011. ^{17}O-depleted barite from two Marinoan cap dolostone sections, South China. Earth Planet. Sci. Lett. 305 (1–2), 21–31. https://doi.org/10.1016/j.epsl.2011.02.014.

Riedinger, N., Kasten, S., Gröger, J., Franke, C., Pfeifer, K., 2006. Active and buried authigenic barite fronts in sediments from the Eastern Cape Basin. Earth Planet. Sci. Lett. 241 (3), 876–887. https://doi.org/10.1016/j.epsl.2005.10.032.

Schlitzer, R., 2011. Ocean Data View.

Shields, G.A., 2005. Neoproterozoic cap carbonates: a critical appraisal of existing models and the plumeworld hypothesis. Terra Nova 17 (4), 299–310. https://doi.org/10.1111/j.1365-3121.2005.00638.x.

Shields, G.A., Deynoux, M., Strauss, H., Paquet, H., Nahon, D., 2007. Barite-bearing cap dolostones of the Taoudéni Basin, northwest Africa: sedimentary and isotopic evidence for methane seepage after a Neoproterozoic glaciation. Precambrian Res. 153 (3–4), 209–235. https://doi.org/10.1016/j.precamres.2006.11.011.

Tivey, M.K., 2007. Generation of seafloor hydrothermal vent fluids and associated mineral deposits. Oceanography 20 (1), 50–65.

Torres, M.E., Bohrmann, G., Suess, E., 1996. Authigenic barites and fluxes of barium associated with fluid seeps in the Peru subduction zone. Earth Planet. Sci. Lett. 144 (3–4), 469–481. https://doi.org/10.1016/S0012-821X(96)00163-X.

Torres, M.E., Bohrmann, G., Dubé, T.E., Poole, F.G., 2003. Formation of modern and Paleozoic stratiform barite at cold methane seeps on continental margins. Geology 31 (10), 897–900. https://doi.org/10.1130/G19652.1.

van Zuilen, K., Müller, T., Nägler, T.F., Dietzel, M., Küsters, T., 2016. Experimental determination of barium isotope fractionation during diffusion and adsorption processes at low temperatures. Geochim. Cosmochim. Acta 186, 226–241. https://doi.org/10.1016/j.gca.2016.04.049.

von Allmen, K., Böttcher, M.E., Samankassou, E., Nägler, T.F., 2010. Barium isotope fractionation in the global barium cycle: first evidence from barium minerals and precipitation experiments. Chem. Geol. 277 (1–2), 70–77.

Wen, J., Thiemens, M.H., 1993. Multi-isotope study of the O(1D)+CO_2 exchange and stratospheric consequences. J. Geophys. Res., Atmos. 98 (D7), 12801–12808.

Yang, J., Jansen, M.F., Macdonald, F.A., Abbot, D.S., 2017. Persistence of a freshwater surface ocean after a snowball Earth. Geology 45 (7), 615–618. https://doi.org/10.1130/G38920.1.

Zhou, C., Bao, H., Peng, Y., Yuan, X., 2010. Timing the deposition of ^{17}O-depleted barite at the aftermath of Nantuo glacial meltdown in South China. Geology 38 (10), 903–906. https://doi.org/10.1130/G31224.1.